



Fast DTI @ 11.7 T: Ready for Cohort Studies

Hans-Peter Müller¹, Ina Vernikouskaya^{2,3}, Albert C. Ludolph¹,
Jan Kassubek¹, Detlef Stiller⁴, Volker Rasche^{2,3}

¹ Department of Neurology, University Hospital Ulm, Ulm, Germany

² Department of Internal Medicine II, University Hospital of Ulm, Ulm, Germany

³ Small Animal MRI, Medical Faculty, University of Ulm, Ulm, Germany

⁴ Target Discovery Research, Boehringer Ingelheim Pharma GmbH&Co. KG, Biberach, Germany

Abstract

The application of the cryogenically cooled resonator enables rapid DTI acquisitions as basis for cohort studies in mice.

Introduction: *in vivo* high resolution diffusion tensor imaging (DTI) of the mouse brain has proven promising application for a variety of pathologies. Its application to large cohort studies, however, is often limited by the intrinsic low signal to noise ratio (SNR) causing long acquisition times. Cryogenically cooled resonators (CCR) have demonstrated the potential for significantly increasing SNR and appear attractive for reducing scan times in DTI imaging thus enabling cohort studies. This contribution describes the DTI acquisition optimization using CCRs and presents the outcome of an initial cohort study at the group level to β -amyloid precursor protein (APP) transgenic mice.

Methods: A DTI sequence providing $156^2 \times 250 \mu\text{m}^3$ spatial resolution with 30 diffusion encoding directions was optimized for using CCR at ultrahigh field (11.7 T), resulting in a total acquisition time of 35 minutes. The quality was directly compared with a standardized 110 minutes acquisition protocol published earlier. Fractional anisotropy (FA) and fiber tracking (FT) results including quantitative tractwise fractional

anisotropy statistics (TFAS) were qualitatively and quantitatively compared. The optimized sequence was then applied to 5 wild type and 7 APP transgenic (tg2576) mice for investigation of its potential for cohort studies. Fractional anisotropy (FA) maps were statistically compared by whole brain-based spatial statistics (WBSS) at the group level vs. wild type controls.

Results: With the optimized protocol no remarkable differences were observed for the qualitative and quantitative assessment of the calculated fractional anisotropy maps and fibre tracking results. Coefficients of variation for ROI-based FA-comparison as well as for TFAS revealed comparable results for the investigated scanning protocols. At the group level, differences were observed between the WT and the transgenic animals at locations associated with Alzheimer's disease in humans, such as the hippocampus, the entorhinal cortex, and the caudoputamen.

Conclusion: DTI of the mouse brain at 11.7 T can be performed within approximately 30 minutes, which renders cohort studies feasible. With the fast protocol reliable and reproducible FA-values and FT reconstructions could be achieved. The application of the fast protocol to cohort studies revealed changes identified by WBSS of the FA maps in regions associated with amyloid- β deposition for the transgenic mice, thus proving the potential of rapid DTI for cohort studies.

Introduction

in vivo as well as *in-vitro* diffusion tensor imaging (DTI) ^[1,2] has evolved as an increasingly important tool for studying the anatomy of the mouse brain ^[1-13]. With DTI mapping of the brain fiber directions and reconstruction of its 3D architecture, rendering axonal tracts and tracking white matter pathways of the human brain is feasible ^[3]. In DTI for each voxel the diffusion tensor of the water protons is assessed ^[1]. Tractography algorithms use this information to track the neural pathways ^[3] enabling to study the anatomical connectivity.

DTI studies of the rodent brain have been reported for different field strength ^[7-13] but still demand long scan times to provide sufficient signal-to-noise ratio (SNR) and spatial resolution. Published acquisition protocols utilize in-plane resolutions between 117 μm and 160 μm with slice thickness between 375 μm and 1 mm with acquisition times ranging up to 1-2 hours ^[11,13]. Even though the spatial resolution revealed acceptable quality to conduct fiber tracking (FT) and consequent tract based spatial statistics (TBSS) ^[6], the related long scanning times limit the application to large cohort studies. For routine pre-clinical application of DTI, further optimization especially regarding reducing acquisition times is mandatory.

The application of cryogenically cooled resonators (CCR) has been proven to enable significant improvement of SNR ^[14,15]. The at least two-fold increase of SNR can be applied for substantial reduction of scan time without sacrificing spatial resolution and should enable high-fidelity DTI information with even decreased slice thickness for improved 3D fiber reconstruction within scan times as short as 30 minutes.

The reduced scan time and well defined DTI information likely enables cohort studies for the analysis of structural changes at the group level. E.g. DTI has been promisingly applied as an imaging correlate to the assessment of human ALZD ^[16,17]. Two major pathologic disorders have been identified: a) accumulation of extracellular amyloid plaques, caused by amyloid- β protein aggregation, and b) the presence of intracellular neurofibrillary tangles, formed by aggregates of the hyperphosphorylated tau protein ^[18]. Changes originate in the medial temporal lobe (entorhinal cortex and hippocampus), spreading across the limbic cortex and neocortex ^[18,19]. Establishing similar biomarkers in preclinical research is currently ongoing ^[20,21]. Here DTI plays an increasingly important role for studying the mouse anatomy ^[22,23]. Previous studies ^[18,24,25] compared different animal groups at subject coordinate space level (e.g. by individual ROI analyses).

The objective of this study was to enable group comparison after stereotaxic normalization on a study-specific template. The feasibility of rapid DTI measurements in cohort studies is shown in APP transgenic mice (APP mice) vs. wild type mice (wt mice). Diffusion related brain differences are identified. The presented work provides the basis for future studies aiming at examining experimental model of ALZD and other neurodegenerative diseases.

Methods and Materials

Animal setup

All experiments were performed in accordance with German animal protection laws and had been approved by the national animal board. The optimized DTI protocol was evaluated in three adult wild type mice (C57/B6, 12 months old). For group comparison seven transgenic mice (tg2576, C57BL6/SJL ^[26], 23 months old) and five adult wild type mice (C57BL/6, 23 months old) were investigated with the optimized protocol.

All data acquisition was performed under isoflurane anesthesia (3% for induction and 1.5% for maintenance). The animals were placed in a stereotactic head support (Bruker Biospin, Ettlingen, Germany). Body temperature was controlled by a water based heating system and monitored by a rectal temperature probe. The breathing frequency was maintained at 75–80 cycles per minute. The mice rapidly recovered (< 5 min) after the termination of anesthesia at the end of the MRI procedure.

Data acquisition

All data was acquired applying a two-element transmit/receive ¹H mouse cryogenic surface coil (CryoProbe, Bruker BioSpin) at 11.7 T (Biospec 117/16, Bruker, Ettlingen, Germany). The rapid DTI protocol ^[29] comprised a diffusion prepared spin echo EPI imaging protocol with acquisition parameters as: TE/TR 50.5 ms / 15000 ms, matrix 128 x 96, in-plane resolution 156 μm x 156 μm , 60 axial slices with a slice thickness of 250 μm . DTI encodings include thirty diffusion directions with $b=1000$ s/mm² and 5 unweighted $b=0$ volumes (standard gradient scheme as provided by the Bruker software). With one signal average and four EPI segments, the total acquisition time resulted as 35 minutes (SP A). For the evaluation of the rapid technique additional measurements were obtained with the protocol as suggested by Harsan et al. ^[11], with acquisition parameter as:

TE/TR 20.5 ms / 7750 ms, matrix 128 x 96, in-plane resolution 156 μm x 156 μm , 30 axial slices with a slice thickness of 500 μm , diffusion scheme identical as before. Six signal averages resulted in a total acquisition time of 110 minutes (SP B). For further assessment of the potential of the CCR, a third protocol identical to SP B with only a single signal average was acquired, resulting in 18 minutes scan time (SP C). No respiratory or cardiac synchronization was used.

Data analysis

Data preprocessing was performed with the Tensor Imaging and Fiber Tracking (TIFT) software package [27]. Fractional anisotropy (FA) maps were calculated and displayed by directional color encoded maps of FA overlaid onto ($b=0$) anatomical images (Figure 2). FA values were compared between the different techniques in three spherical volumes located the septohippocampal nucleus, the corpus callosum, and in the medial septal nucleus. Major pathways were identified by FT with seed points located at the genu and along the corpus callosum, near the lateral septal nucleus, and in the olfactory tract (Figure 3). Quality of the tractography was assessed by tractwise fractional anisotropy statistics (TFAS) [28].

For group analysis, iterative spatial normalization to a stereotaxic standard space was performed using a study-specific b_0 -template and an FA-template [30]. Scanner- and sequence specific b_0 - and FA-templates were created averaging data sets of all mice after linear transformation according to manually identified landmarks according to a stereotaxic mouse atlas [31]. The flow chart of the whole brain-based spatial statistics is provided in Figure 5. A recently published quality procedure [32] was applied for reduction of motion artifacts. DTI metrics were calculated according to current standard methods [33]. For a more detailed description, please refer to Mueller et al [30].

Results

For the suggested segmented EPI sequence, application of the two-element cryogenic brain resulted in an average gain in SNR over the brain by a factor of 2.3 with peak values close to 3, when compared to the four-element phased-array coil (Figure 1).

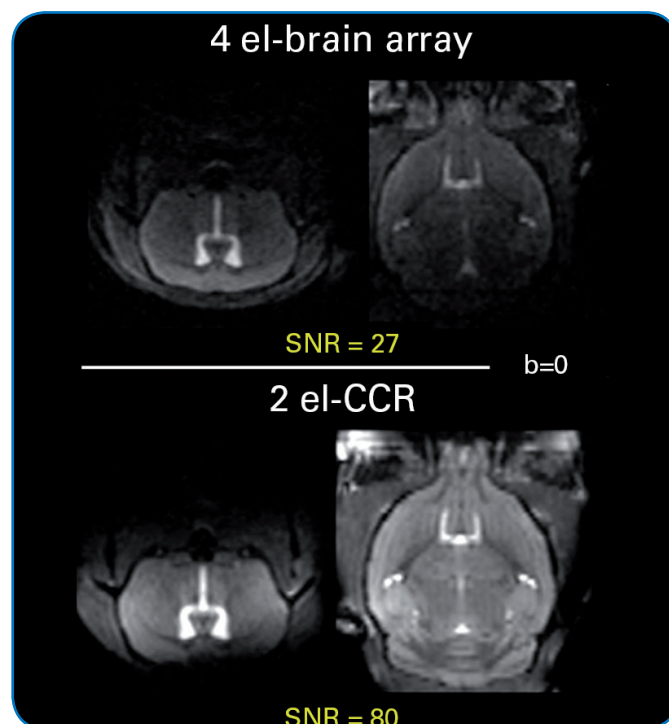


Figure 1: Four-element brain array coil (top) vs. two-element cryogenic cooled resonator (CCR – bottom) Anatomic images (axial slice and coronal reconstruction) used for signal-to-noise ratio (SNR) calculations.

A representative slice of the color-coded FA map reconstructed in coronal orientation is presented in Figure 2. The quality of the 18 min scan (SP C) with 500 μm slice thickness appears similar to the 110 min protocol (SP B). Decreasing the slice thickness (SP A) yields improved delineation of the axial structures.

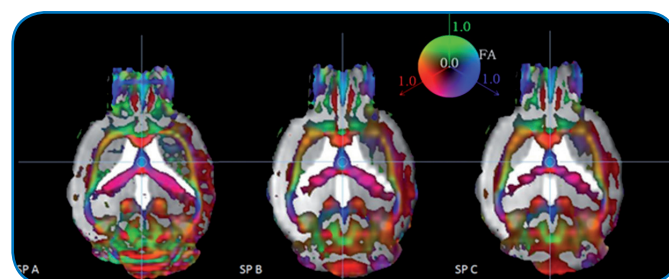


Figure 2: Directional encoded color maps of FA overlaid to anatomical images reconstructed in coronal slice orientation. Scanning protocols SP A (35 minutes, 1 average, 250 μm slice thickness), SP B (110 minutes, 6 averages, 500 μm slice thickness, protocol according to [13]), and SP C (18 minutes, 1 average, 500 μm slice thickness, protocol according to [13] but with CCR and optimized acquisition time).

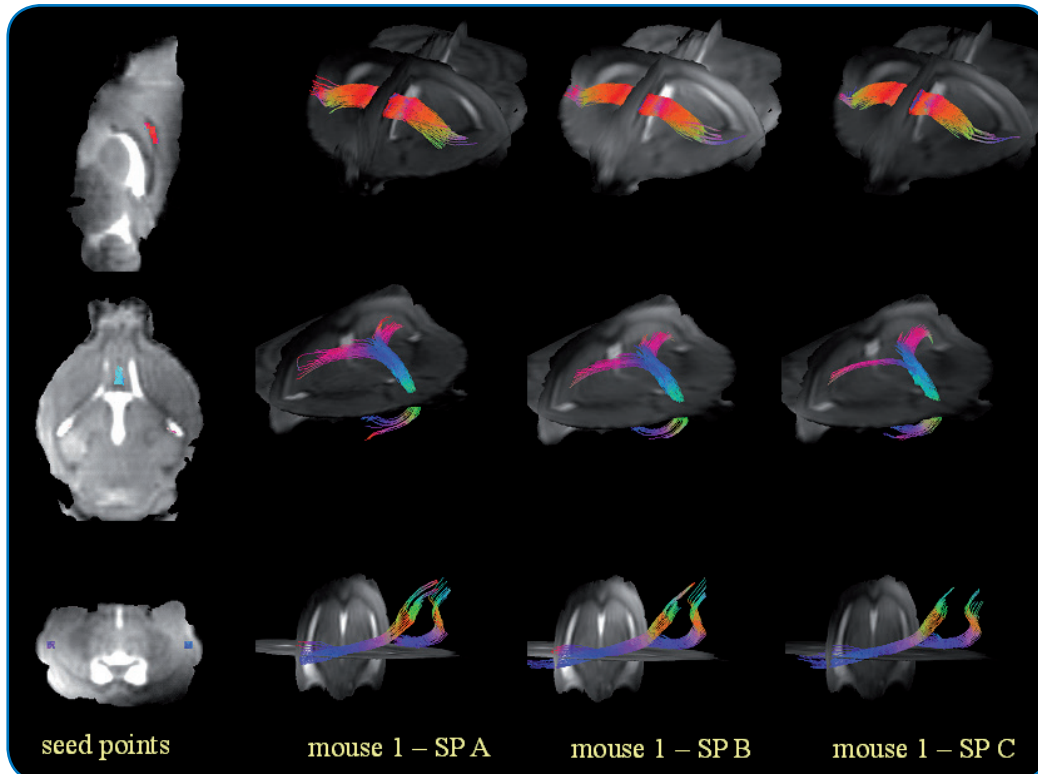


Figure 3: FT results for seed points in the genu and along the corpus callosum, near the lateral septal nucleus, and in the olfactory path (left). Exemplary FT with different scanning protocols (SP A-C).

Resulting tractography results with respective seed points are shown in Figure 3. Quantitative comparison of the FA values and TFAS yielded high reproducibility of the results between the different mice. Observed FA values were slightly higher in the rapid high-resolution protocol (SP A). TFAS and coefficient of variance (CV) revealed almost identical values.

The application of the rapid scan protocol for the cohort analysis revealed significant alteration of the FA values between APP and wt mice. A widespread characteristic and symmetric pattern of FA differences was revealed by whole brain-based spatial statistics (WBSS). FA reduction in APP mice was observed in caudoputamen, the dorsal hippocampus, the entorhinal cortex, the thalamus, internal capsules, paramedian raphe nucleus area and in the periaqueductal grey. Increased FA values were observed near the lateral septal nucleus area and the ventral ventricles, and in the lateral cerebellum. Further observed differences include significant signal reduction in mean diffusivity (MD; lateral septal nucleus area, dorsal hippocampus, amygdale, and internal capsule), reduction of axial diffusivity (AD; bilaterally in the dorsal hippocampus and the entorhinal cortex, dorsomedial hypothalamic nucleus, lateral septal nucleus), and radial diffusivity (RD; bilaterally in the cerebellum and the dentate gyrus, lateral septal nucleus and in the thalamus region). Exemplary results for the lateral septal nucleus are shown in Figure 4.

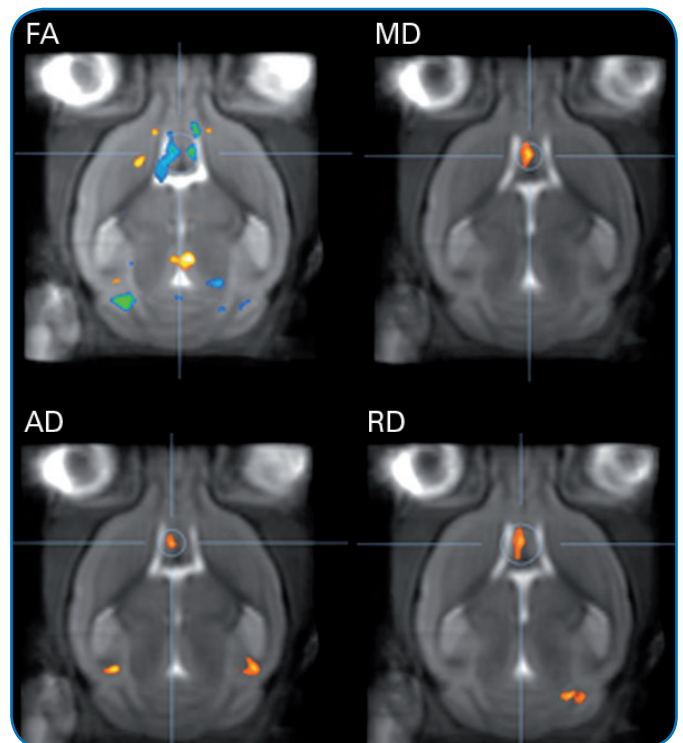


Figure 4: Results from whole brain-based spatial statistics (WBSS) of FA-, MD-, AD-, and RD-maps of APP mice vs. wt mice at $p < 0.05$, exemplarily shown for the lateral septal nucleus.

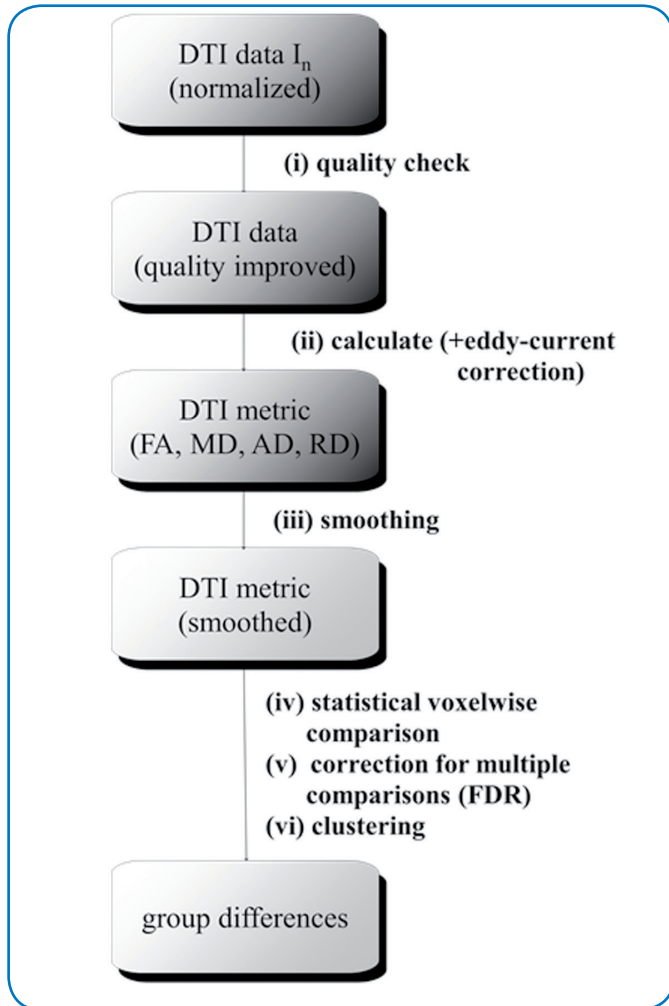


Figure 5: Workflow of the whole brain-based spatial statistics (WBSS). After a quick quality check (i) to eliminate motion corrupted volumes, eddy-current correction was performed prior to DTI-metrics calculation (ii). Smoothing of the DTI-metrics maps (iii), statistical voxelwise comparison (iv), correction for multiple comparisons (v), and clustering (vi) lead to significant group differences.

Conclusions

We could show that using a two-element cryogenically cooled resonator (CCR) enables *in vivo* fiber tracking and microstructural analysis of the mouse brain with high spatial definition based on MRI DTI data acquired in about 35 minutes. The average SNR improvement of a factor of 2.3 with the CCR enabled DTI scans with only a single signal average and provides the opportunity to accurately calculate diffusion tensors and FA-maps yielding reliable FA-values and FT reconstructions. For high-resolution FT, small preferably isotropic voxels are paramount. With the presented protocol, spatial resolutions in the order of axon bundles could be achieved. Sufficient spatial resolution was provided for enabling the use of post-processing technique well known from human group studies. Slight differences in the FA values may be attributed to the higher spatial resolution and the resulting less averaging over axons or the reduction of partial volume

effects especially in the vicinity of white matter or CSF.

The experimental setup of this study allows for *in vivo* large scale whole brain murine DTI cohort studies as shown in the presented investigation of structural brain changes at the group level. The rapid imaging protocol at 11.7 T ensured sufficient image quality for subsequent analysis at the group level by WBSS. Significant differences in the FA values between wt and APP mice could already be observed in small animal cohorts. The identified bilateral DTI metric alterations in the dorsal hippocampus and in the entorhinal cortex may suggest axonal injury. Myelin degeneration in not coherently aligned fiber structures may cause FA increase in the cerebellum combined with RD decrease. The small but significant bilateral RD decrease in the dentate gyrus is not understood and should be topic to further research.

Interestingly, the regions with identified FA alterations (i.e. hippocampus and entorhinal cortex) were mainly related to anatomical structures already identified as ALZD related in human DTI studies. Other alteration (thalamus, internal capsule, and hippocampus) have also been identified by DTI studies in mice. Further regions being likely associated with ALZD were identified, e.g. the caudoputamen, as well as the thalamus and the raphe nuclei.

Even though the current study at the group level is still limited by the small number of animals enrolled and no histological workup, we believe that the hemispherical symmetry of the FA alterations indicates a high reliability of the achieved results.

The single signal average used for the fast DTI imaging protocol may be prone to motion artifacts. With the suggested technique for detection and elimination of motion corrupted volumes, we did not experience any severe limitations in cases where up to 10 directions have to be excluded from further analysis. Motion artifacts might be addressed by cardiac and respiratory gating. Initial experiments did only show slight to no improvement in image quality while substantially sacrificing image acquisition time. Therefore automatic identification of corrupted volumes may be sufficient.

References

- [1] Bassler PJ, Mattiello J, LeBihan D (1994) MR diffusion tensor spectroscopy and imaging. *Biophys J* 66: 259–267.
- [2] Mori S, Zhang J (2006) Principles of diffusion tensor imaging and its applications to basic neuroscience research. *Neuron* 51: 527–539.
- [3] Chuang N, Mori S, Yamamoto A, Jiang H, Ye X, et al. (2011) An MRI-based atlas and database of the developing mouse brain. *Neuroimage* 54: 80–89.
- [4] Gutman DA, Keifer OP Jr, Magnuson ME, Choi DC, Majeed W, et al. (2012) A DTI tractography analysis of infralimbic and prelimbic connectivity in the mouse using high-throughput MRI. *Neuroimage* 63: 800–811.
- [5] Pathak AP, Kim E, Zhang J, Jones MV (2011) Three-dimensional imaging of the mouse neurovasculature with magnetic resonance microscopy. *PLoS One* 6: e22643.
- [6] Ruest T, Holmes WMM, Barrie JA, Griffiths IR, Anderson TJ, et al. (2011) High-resolution diffusion tensor imaging of fixed brain in a mouse model of Pelizaeus-Merzbacher disease: comparison with quantitative measures of white matter pathology. *NMR Biomed* 24: 1369–1379.
- [7] Boretius S, Würfel J, Zipp F, Frahm J, Michaelis T (2007) High-field diffusion tensor imaging of mouse brain *in vivo* using single-shot STEAM MRI. *J Neurosci Methods* 161: 112–117.
- [8] Guilfoyle DN, Gerum S, Hrabe J (2011) Murine diffusion imaging using snapshot interleaved EPI acquisition at 7T. *J Neurosci Methods* 199: 10–14.
- [9] Jiang Y, Johnson GA (2011) Microscopic diffusion tensor atlas of the mouse brain. *Neuroimage* 56: 1235–1243.
- [10] Kumar M, Kim S, Pickup S, Chen R, Fairless AH, et al. (2012) Longitudinal *in vivo* diffusion tensor imaging for assessing brain developmental changes in BALB/cJ mouse, a model of reduced sociability relevant to autism. *Brain Res* 1455: 56–67.
- [11] Harsan LA, Paul D, Schnell S, Kreher BW, Hennig J, et al. (2010) *in vivo* diffusion tensor magnetic resonance imaging and fiber tracking of the mouse brain. *NMR Biomed*. 23: 884–896.
- [12] Aggarwal M, Zhang J, Miller MI, Sidman RL, Mori S (2009) Magnetic resonance imaging and micro-computed tomography combined atlas of developing and adult mouse brains for stereotaxic surgery. *Neuroscience* 162: 1339–1350.
- [13] Aggarwal M, Mori S, Shimogori T, Blackshaw S, Zhang J (2010) Three-dimensional diffusion tensor microimaging for anatomical characterization of the mouse brain. *Magn Reson Med* 64: 249–261.
- [14] Ratering D, Baltes C, Nordmeyer-Massner J, Marek D, Rudin M (2008) Performance of a 200-MHz cryogenic RF probe designed for MRI and MRS of the murine brain. *Magn Reson Med* 59: 1440–1447.
- [15] Baltes C, Radzwill N, Bosshard S, Marek D, Rudin M (2009) Micro MRI of the mouse brain using a novel 400 MHz cryogenic quadrature RF probe. *NMR Biomed* 22: 834–842.
- [16] Ota M, Sato N, Nakata Y, Arima K, Uno M (2012) Relationship between apathy and diffusion tensor imaging metrics of the brain in Alzheimer's disease. *Int J Geriatr Psychiatry* 27: 722–726.
- [17] Stebbins GT and Murphy CM (2009) Diffusion tensor imaging in Alzheimer's disease and mild cognitive impairment. *Behav Neurol* 21: 39–49.
- [18] Zerbi V, Kleinnijenhuis M, Fang X, Jansen D, Veltien A, et al. (2012) Gray and white matter degeneration revealed by diffusion in an Alzheimer mouse model. *Neurobiol Aging* doi:pii: S0197-4580(12)00594-5. 10.1016/.
- [19] Braak H, Braak E (1995) Staging of Alzheimer's disease-related neurofibrillary changes. *Neurobiol. Aging* 16, 271–278; discussion 278–284.
- [20] Jack Jr CR, Garwood M, Wengenack TM, Borowski B, Curran GL, et al. (2004) *in vivo* visualization of Alzheimer's amyloid plaques by magnetic resonance imaging in transgenic mice without a contrast agent. *Magn Reson Med* 52: 1263–1271.
- [21] Delatour B, Guegan M, Volk A, Dhenain M (2006) *in vivo* MRI and histological evaluation of brain atrophy in APP/PS1 transgenic mice. *Neurobiol Aging* 27: 835–847.
- [22] Harsan LA, Paul D, Schnell S, Kreher BW, Hennig J, et al. (2010) *in vivo* diffusion tensor magnetic resonance imaging and fiber tracking of the mouse brain. *NMR Biomed*. 23: 884–896.
- [23] Aggarwal M, Mori S, Shimogori T, Blackshaw S, Zhang J (2010) Three-dimensional diffusion tensor microimaging for anatomical characterization of the mouse brain. *Magn Reson Med* 64: 249–261.
- [24] Sun SW, Song SK, Harms MP, Lin SJ, Holtzman DM, et al. (2005) Detection of age-dependent brain injury in a mouse model of brain amyloidosis associated with Alzheimer's disease using magnetic resonance diffusion tensor imaging. *Exp Neurol* 191: 77–85.
- [25] Song SK, Kim JH, Lin SJ, Brendza RP, Holtzman DM (2004) Diffusion tensor imaging detects age-dependent white matter changes in a transgenic mouse model with amyloid deposition. *Neurobiol Dis* 15: 640–647.
- [26] Hsiao K, Chapman P, Nilsen S, Eckman C, Harigaya Y, et al. (1996) Correlative memory deficits, Aβ elevation, and amyloid plaques in transgenic mice. *Science* 274: 99–102.
- [27] Müller HP, Unrath A, Ludolph AC, Kassubek J (2007) Preservation of diffusion tensor properties during spatial normalization by use of tensor imaging and fibre tracking on a normal brain database. *Phys Med Biol* 52: N99–109.
- [28] Müller HP, Unrath A, Sperfeld AD, Ludolph AC, Riecker A, et al. (2007) Diffusion tensor imaging and tractwise fractional anisotropy statistics: quantitative analysis in white matter pathology. *Biomed Eng Online* 6: 42.
- [29] Mueller HP, Vernikouskaya I, Kassubek J, Rasche V. Fast diffusion tensor magnetic resonance imaging of the mouse brain with a cryogenic coil at ultrahigh-field: optimization of the scanning protocol enables acquisition times useful for cohort studies. *PLoS One*. 2012;7(12):e53389.
- [30] Mueller HP, Vernikouskaya I, Kassubek J, Ludolph AC, Stiller D, Rasche V. Diffusion tensor magnetic resonance imaging of the brain in APP transgenic mice: a cohort study. *PlosOne* 2013;8(6):e67630.
- [31] Paxinos G and Franklin KBJ (2007) The mouse brain in stereotaxic coordinates. Academic press. Elsevier 3rd ed.
- [32] Müller HP, Süßsmuth SD, Landwehrmeyer GB, Ludolph A, Tabrizi SJ, et al. (2011) Stability effects on results of diffusion tensor imaging analysis by reduction of the number of gradient directions due to motion artifacts: an application to presymptomatic Huntington's disease. Version 2. *PLoS Curr* 3: RRN1292.
- [33] Bassler PJ, Jones DK (2002) Diffusion-tensor MRI: theory, experimental design and data analysis - a technical review. *NMR Biomed* 15, 456–467.